







Enhanced thermal stability of yttrium oxide-based RRAM devices with inhomogeneous Schottky-barrier

Cite as: Appl. Phys. Lett. **117**, 013504 (2020); <https://doi.org/10.1063/5.0009645>

Submitted: 01 April 2020 . Accepted: 20 June 2020 . Published Online: 10 July 2020

Eszter Piros , Stefan Petzold , Alexander Zintler , Nico Kaiser , Tobias Vogel , Robert Eilhardt 
, Christian Wenger , Leopoldo Molina-Luna , and Lambert Alff 



View Online



Export Citation



CrossMark

Lock-in Amplifiers
up to 600 MHz



Enhanced thermal stability of yttrium oxide-based RRAM devices with inhomogeneous Schottky-barrier

Cite as: Appl. Phys. Lett. **117**, 013504 (2020); doi: 10.1063/5.0009645

Submitted: 1 April 2020 · Accepted: 20 June 2020 ·

Published Online: 10 July 2020



View Online



Export Citation



CrossMark

Eszter Piros,^{1,a)}  Stefan Petzold,¹  Alexander Zintler,²  Nico Kaiser,¹  Tobias Vogel,¹  Robert Eilhardt,²  Christian Wenger,^{3,4}  Leopoldo Molina-Luna,²  and Lambert Alff¹ 

AFFILIATIONS

¹Advanced Thin Film Technology Division, Institute of Materials Science, Technische Universität Darmstadt, Alarich-Weiss-Str. 2, 64287 Darmstadt, Germany

²Advanced Electron Microscopy Division, Institute of Materials Science, Technische Universität Darmstadt, Alarich-Weiss-Str. 2, 64287 Darmstadt, Germany

³IHP-Leibniz-Institut für Innovative Mikroelektronik, Im Technologiepark 25, 15236 Frankfurt (Oder), Germany

⁴Brandenburg Medical School Theodor Fontane, Fehrbelliner Str. 38, 16816 Neuruppin, Germany

^{a)} Author to whom correspondence should be addressed: eszter.piros@tu-darmstadt.de

ABSTRACT

This work addresses the thermal stability of bipolar resistive switching in yttrium oxide-based resistive random access memory revealed through the temperature dependence of the DC switching behavior. The operation voltages, current levels, and charge transport mechanisms are investigated at 25 °C, 85 °C, and 125 °C, and show overall good temperature immunity. The set and reset voltages, as well as the device resistance in both the high and low resistive states, are found to scale inversely with increasing temperatures. The Schottky-barrier height was observed to increase from approximately 1.02 eV at 25 °C to approximately 1.35 eV at 125 °C, an uncommon behavior explained by interface phenomena.

© 2020 Author(s). All article content, except where otherwise noted, is licensed under a Creative Commons Attribution (CC BY) license (<http://creativecommons.org/licenses/by/4.0/>). <https://doi.org/10.1063/5.0009645>

Resistive Random Access Memory (RRAM) devices have been gaining increasing interest in the past decades as an alternative for the existing technologies in non-volatile memory applications¹ and as low-device-area synaptic elements for neuromorphic computing.² The attractiveness of RRAM lies in its great scaling potential,³ demonstrated high endurance,⁴ sub-nanosecond read/write speed,^{5,6} and potential low-power operation.⁷ In devices that work based on the valence change mechanism (VCM), the basic operation principle is the change of resistance through the controlled and reversible dielectric breakdown of the oxide layer, during which a defect-rich conducting path called conductive filament (CF) forms. Upon the application of appropriate voltage or current, the cell can be switched between a low (LRS) and a high resistive state (HRS). The very first breakdown (initial CF formation) is called the electroforming process; otherwise, the HRS-to-LRS transition is referred to as “set,” while the opposite process as “reset.” The biggest limitations that have to be overcome for RRAM lie in device reliability and variability. Thus, it is important to

investigate and understand the stability of the performance parameters under external stress, e.g., radiation effects⁸ or at elevated temperatures, and to gain insight into the physical mechanisms that govern charge transport processes in the HRS as well as in the LRS. Many possible mechanisms have been proposed for conduction in both resistive states,⁹ partly due to the large variety of materials used as electrodes and functional layers in RRAM, highlighting the importance of appropriate material choice. Yttrium oxide-based RRAM is a fairly new and promising non-volatile memory^{10–12} and an artificial synapse candidate.^{12,13} Yttria was considered as an alternative to SiO₂ as a gate oxide material in CMOS applications because of its high dielectric constant, large bandgap, and good thermal stability.^{14,15} Unlike other transition metal oxides exploited as the functional layer in RRAM, such as hafnium or tantalum oxide, for yttria the only stable stoichiometry is Y₂O₃.¹⁶ It has been shown that oxygen engineering of the functional layer in hafnia-based RRAM is beneficial in lowering the operation voltages due to a high oxygen vacancy density.^{17,18} In the case of

yttrium oxide, however, the high oxygen defect concentration is intrinsic to the crystal structure even in the stoichiometric compound, resulting in uniform resistive switching and electronic noise characteristics.¹⁹ The cubic *C*-type fluorite, also known as the sesquioxide or bixbyite structure of Y_2O_3 , is inherently rich in defects as the occupation of the anion sublattice sites is only 75%, giving rise to structural oxygen vacancies²⁰ and making yttria an interesting material for oxygen and defect migration-based RRAM applications.

In this work, we report on the enhanced thermal stability and strongly reduced device-to-device and cycle-to-cycle variability of yttria-based RRAM. It is shown that, compared to the highly investigated hafnium oxide or tantalum oxide-based VCM-type systems, RRAM based on yttrium oxide shows very uniform switching characteristics. The operation voltages as well as the HRS and LRS current levels exhibit high uniformity, also at elevated temperatures. The observed characteristics are ascribed to the intrinsic high oxygen defect density in yttria. Additionally, the modification of the Schottky-barrier height with increasing temperature is reported. This phenomenon is of high importance as a better understanding of device physics is inevitable for the successful integration of RRAM.

The fabrication details of the devices under test (DUTs) consisting of TiN/ Y_2O_3 /Pt are described in our previous work.¹² A Keithley 4200 semiconductor characterization system (SCS) was used to carry out the electrical measurements. A voltage bias was applied to the Pt top electrode while keeping the TiN bottom electrode grounded. The internal current compliance (CC) of the SCS was used to inhibit the hard dielectric breakdown of the oxide layer. A LakeShore 336 temperature controller was used for the temperature-dependent characterization. Scanning transmission electron microscopy images were obtained by using a JEOL JEM ARM-200F.

Figures 1(a) and 1(b) show the high-angle annular dark-field scanning transmission electron microscopy (HAADF-STEM) overview of the whole thin film stack and of the yttria layer, respectively. Through the high-resolution contrast, individual grains can be visualized in the polycrystalline structure of the Y_2O_3 film. The TiN/ Y_2O_3 interface appears to be blurred, which might be due to the formation of an interfacial layer consisting of TiO_x or more likely of TiO_xN_{x-1} .²¹ It is known that ohmic electrodes with high oxygen affinity are prone to oxidize upon contact with an oxide, which in turn results in the reduction of the insulating matrix.²² The formation of such an interfacial layer can assist the switching process by creating oxygen vacancies in the oxide layer and serving as an oxygen reservoir during reset. To assess the impact of temperature on the electrical behavior, six devices were pre-cycled at room temperature in ambient conditions in order to activate the resistive switching property. The measurements at elevated temperatures were carried out in vacuum. As reported in our previous work,¹² the devices are electroforming-free. In Fig. 1(c), representative $I - V$ characteristics are shown under DC voltage sweep operation ($V_{sweep, set} = -2.5$ V and $V_{sweep, reset} = +2.5$ V) at 25 °C, 85 °C, and 125 °C for one of the DUTs. The observed bipolar resistive switching behavior has been attributed to the valence change mechanism,¹² where the CF formation and rupture are related to the electric field-driven motion of anions, commonly described in literature by oxygen vacancy migration. The resistive switching effect is then related to the local reduction and oxidation of the CF.

Charge transport in both resistive states has been tested for several mechanisms by the evaluation of the $I - V$ curves recorded at the

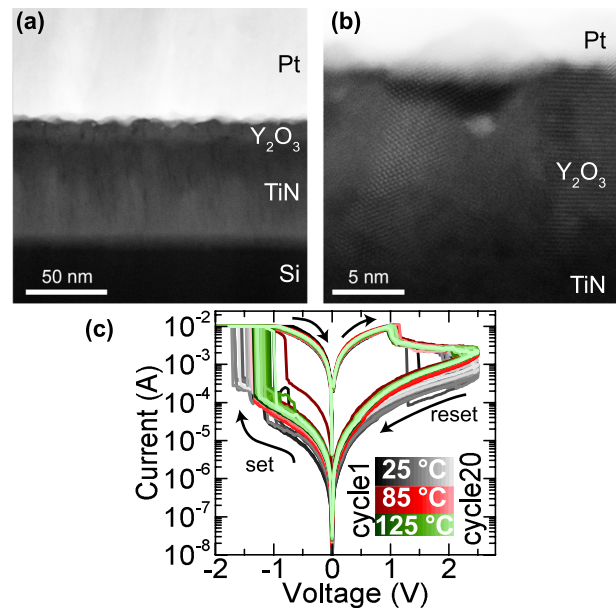


FIG. 1. (a) HAADF-STEM image of the whole device stack. (b) HAADF-STEM image of the Y_2O_3 thin film. Through high-resolution contrast, individual grains can be identified. (c) Bipolar resistive switching current–voltage characteristics of yttria-based RRAM at 25 °C, 85 °C, and 125 °C. The current levels slightly shift to higher values with increasing temperature.

three measurement temperatures. These include the space-charge-limited conduction (SCLC), Poole–Frenkel emission, ionic and ohmic conduction, Schottky-emission, nearest neighbor hopping (NNH) and variable-range hopping (VRH), and well as trap-assisted tunneling (TAT).⁹ In previous results on yttria-based RRAM,^{10,12} the conduction mechanism in the LRS was identified to follow ohmic behavior, whereas the HRS was described by the Schottky-emission. This has been confirmed now also at higher temperatures as shown in Figs. 2(a) and 2(b), for the LRS and the HRS conduction, respectively. The Schottky-emission is described by²³

$$I = AT^2 \exp \{ (\beta V^{1/2} - \Phi_B) (k_B T)^{-1} \}, \quad (1)$$

$$\beta = (e^3 / 4\pi\epsilon_0\epsilon_r)^{1/2}, \quad (2)$$

where A , T , Φ_B , k_B , e , ϵ_0 , and ϵ_r are the Richardson constant, the absolute temperature, the effective barrier height, Boltzmann's constant, the elementary charge, the permittivity of free space, and the relative permittivity, respectively. The indicator for the formation of a Schottky-contact can be the observation of rectifying characteristics. In the investigated devices such behavior was found as under opposite bias the current-voltage curves are asymmetric. As can be seen from (1) and (2), for Schottky-emission, the $\ln(I/T^2)$ vs $V^{1/2}$ plot has to show a linear dependence, which is fulfilled in our case for the higher voltage region [Fig. 2(b)]. Moreover, the effective Schottky-barrier height Φ_B can also be obtained and is plotted as a function of temperature in Fig. 2(c). The effective barrier height, associated with the Y_2O_3 /Pt interface, was found to increase with increasing temperature from ~ 1.02 eV at 25 °C to ~ 1.35 eV at 125 °C. This phenomenon has been occasionally observed in inhomogeneous Schottky-diodes^{24,25} and was

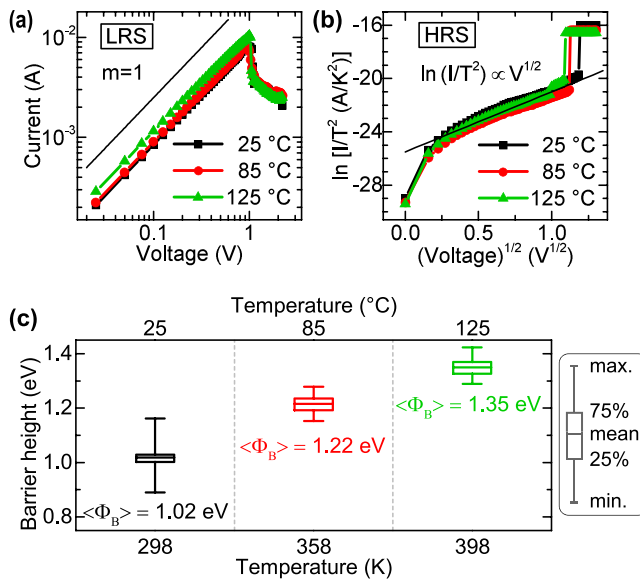


FIG. 2. (a) Ohmic conduction of the LRS and (b) Schottky-emission dominated charge transport in the HRS. The black lines serve as guide to the eye with a slope of 1 and 4.5 for the LRS and HRS, respectively. (c) Box plots of the calculated Schottky-barrier height for six measured devices at 25 °C, 85 °C, and 125 °C.

usually attributed to specific interface phenomena,^{26,27} such as charges at the interface, surface roughness, defects, etc. These imperfections at the interface locally modify the barrier profile, which then cannot be described with a single value of the barrier height, resulting in an inhomogeneous spatial distribution of the latter. Thus, at low temperatures, the highest probability of successful electron transport is at the lowest barriers. However, with increasing temperature, the number of electrons which have sufficient energy to overcome the higher barriers increases, which in turn results in the observed increase in the effective barrier height.²⁸ In the present case, a plausible reason for this inhomogeneity can be the rough Y₂O₃/Pt interface as visible in Figs. 1(a) and 1(b) as well as the polycrystallinity of the yttria layer showing a coexistence of two cubic phases with (222) and (400) orientation and a monoclinic (40 $\bar{2}$) phase as revealed by x-ray diffraction measurements.¹² Also, the possibility of point defects at the interface modifying the barrier profile cannot be excluded.

In Fig. 3(a), the resistance distributions of the HRS and LRS are shown as a function of temperature for all measured devices ($V_{\text{read}} = -0.2 \text{ V}$). Note that for each device and at each temperature, at least twenty DC cycles were carried out, i.e., at least 120 measurement points are included in the statistical analysis shown in Figs. 3(a) and 3(b) for each temperature value. For both resistance states, a semi-conducting behavior was observed, i.e., the resistance decreases with increasing temperature. This excludes the possibility of information storage via a metallic filament as in Conducting Bridge RAM/Electrochemical Metallization Memories. The standard deviation of the resistance values is reduced at higher temperatures. Both resistive states exhibit good thermal stability as no enhanced degradation can be observed of either the HRS or the LRS resistance. In our previous study, we have also shown that the devices exhibit good retention characteristics in the ten year extrapolation at 85 °C and ambient pressure.¹²

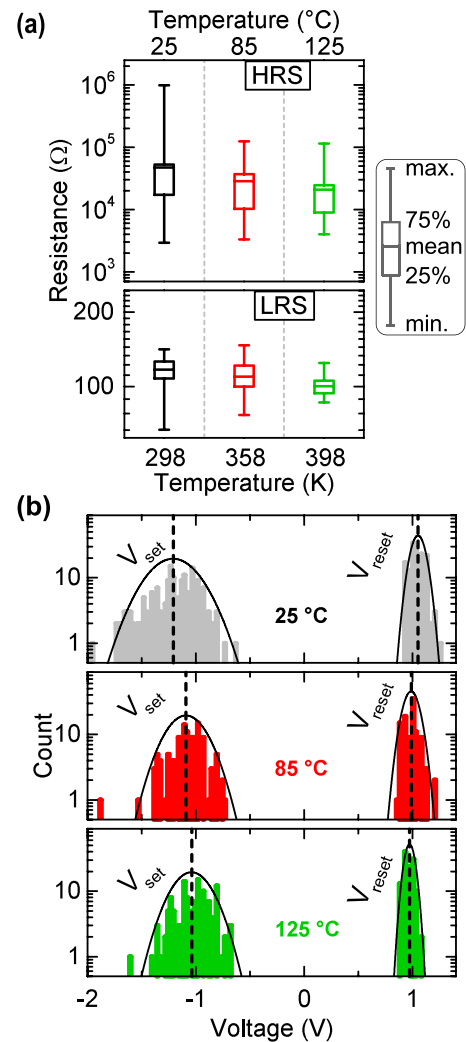


FIG. 3. (a) Box plots of HRS (top) and LRS (bottom) resistance of 6 devices at the measurement temperatures, $V_{\text{read}} = -0.2 \text{ V}$; (b) set (left) and reset (right) voltage cumulative distribution statistics of six devices at 25 °C, 85 °C, and 125 °C.

In Fig. 3(b), the set and reset voltage distributions are shown cumulatively for all DUTs. The reset voltage is defined here as the voltage where the LRS current starts to decrease. We find very low operation voltages at all temperatures with $V_{\text{set}} < 2 \text{ V}$ and $V_{\text{reset}} \approx 1 \text{ V}$. Both V_{set} and V_{reset} exhibit low device to device variation as indicated by the small data spread. A higher uniformity and a shift to lower voltages with increasing temperature were observed, which is more pronounced in the case of V_{set} . Similar behavior was found in TaO_x,²⁹ as well as in HfO₂-based devices and has been related to the increased mobility of oxygen ions and the higher probability of creating oxygen vacancies at increased temperatures.³⁰ In the case of the yttria-based devices, we find that the change of the HRS and LRS resistance as well as of V_{set} and V_{reset} is strongly reduced in comparison to the hafnia and tantalum oxide-based devices. This, including the low operation voltages, can be understood to be consequential to the inherent

abundance of oxygen vacancies in yttrium oxide.^{20,31} As already mentioned, these so-called constitutional oxygen vacancies are intrinsic to the crystal structure and form non-intersecting channels in the oxide, which can serve as low energy ion migration paths,¹⁶ thus facilitating filament formation. This in turn leads to uniform switching characteristics and reduced inter- and intradevice variability.

In conclusion, the operation voltages and the resistance window in Y_2O_3 -based RRAM show high thermal stability at elevated temperatures. Investigating the temperature dependence of the electrical characteristics revealed that the distribution of the set and reset voltages as well as the high and low resistive state resistances becomes narrower with increasing temperature. For all devices and test temperatures, the operation voltage window was found to span from $-2V$ to $1V$. It has been confirmed that resistive switching in the investigated devices is based on the valence change mechanism as both resistive states exhibit semiconducting behavior. The LRS charge transport shows ohmic conduction, whereas the HRS conduction is characterized by Schottky-emission. The obtained effective Schottky-barrier height was found to increase from ~ 1.02 eV at $25^\circ C$ to ~ 1.35 eV at $125^\circ C$ and has been associated with barrier height inhomogeneity at the interface.

This work was supported by the Deutscher Akademischer Austauschdienst (DAAD) and the Deutsche Forschungsgemeinschaft under Project No. AL 560/21-1. The authors gratefully acknowledge financial support by the Federal Ministry of Education and Research (BMBF) under Contract Nos. 16ES0250 and 16ESE0298 and by ENIAC JU within the project PANACHE. This work has been undertaken in the framework of the WAKeMeUP project which received funding from the Electronic Components and Systems for European Leadership Joint Undertaking in collaboration with the European Union's H2020 Framework Programme (H2020/2014-2020) and National Authorities, under Grant Agreement No. 783176. Also, funding from DFG Grant No. MO 3010/3-1 and the European Research Council (ERC) "Horizon 2020" Program under Grant No. 805359-FOXON is gratefully acknowledged.

DATA AVAILABILITY

The data that support the findings of this study are available from the corresponding author upon reasonable request.

REFERENCES

- R. Waser, R. Dittmann, C. Staikov, and K. Szot, "Redox-based resistive switching memories nanoionic mechanisms, prospects, and challenges," *Adv. Mater.* **21**, 2632–2151 (2009).
- D. Ielmini, "Brain-inspired computing with resistive switching memory (RRAM): Devices, synapses and neural networks," *Microelectron. Eng.* **190**, 44–53 (2018).
- K.-S. Li, C. Ho, M.-T. Lee, M.-C. Chen, C.-L. Hsu, J. M. Lu, C. H. Lin, C. C. Chen, B. W. Wu, Y. F. Hou, C. Y. Lin, Y. J. Chen, T. Y. Lai, M. Y. Li, I. Yang, C. S. Wu, and F.-L. Yang, "Utilizing sub-5 nm sidewall electrode technology for atomic-scale resistive memory fabrication," in Symposium on VLSI Technology (VLSI-Technology)-Digest of Technical Papers (2014), pp. 1–2.
- K. Chang, R. Zhang, T.-C. Chang, T. Tsai, T.-J. Chu, H.-L. Chen, C.-C. Shih, C.-H. Pan, Y.-T. Su, P.-J. Wu, and S. M. Sze, "High performance, excellent reliability multifunctional graphene oxide doped memristor achieved by self-protective compliance current structure," in IEEE International Electron Devices Meeting (2014), pp. 33.3.1–33.3.4.
- A. C. Torrezan, J. P. Strachan, G. Medeiros-Ribeiro, and R. S. Williams, "Subnanosecond switching of a tantalum oxide memristor," *Nanotechnology* **22**, 485203 (2011).
- B. J. Choi, A. C. Torrezan, J. P. Strachan, P. G. Kotula, A. J. Lohn, M. J. Marinella, Z. Li, R. S. Williams, and J. J. Yang, "High-speed and low-energy nitride memristors," *Adv. Funct. Mater.* **26**, 5290–5296 (2016).
- C.-F. Kang, W.-C. Kuo, W. Bao, C.-H. Ho, C.-W. Huang, W.-W. Wu, Y.-H. Chu, J.-Y. Juang, S. H. Tseng, L. Hu, and J.-H. He, "Self-formed conductive nanofilaments in (Bi, Mn)Ox for ultralow-power memory devices," *Nano Energy* **13**, 283–290 (2015).
- S. Petzold, S. U. Sharath, J. Lemke, E. Hildebrandt, C. Trautmann, and L. Alff, "Heavy ion radiation effects on hafnium oxide-based resistive random access memory," *IEEE Trans. Nucl. Sci.* **66**, 1715–1718 (2019).
- E. Lim and R. Ismail, "Conduction mechanism of valence change resistive switching memory: A survey," *Electronics* **4**, 586–613 (2015).
- T.-M. Pan, K.-M. Chen, and C.-H. Lu, "Resistive switching behavior in the Ru/ Y_2O_3 /TaN nonvolatile memory device," *Electrochem. Solid-State Lett.* **14**, H27–H29 (2011).
- C. Pi, Y. Ren, Z. Q. Liu, and W. K. Chim, "Unipolar memristive switching in yttrium oxide and RESET current reduction using a yttrium interlayer," *Electrochem. Solid-State Lett.* **15**, G5 (2012).
- S. Petzold, E. Piros, S. U. Sharath, A. Zintler, E. Hildebrandt, L. Molina-Luna, C. Wenger, and L. Alff, "Gradual reset and set characteristics in yttrium oxide based resistive random access memory," *Semicond. Sci. Technol.* **34**, 075008 (2019).
- M. Das, A. Kumar, R. Singh, M. T. Htay, and S. Mukherjee, "Realization of synaptic learning and memory functions in Y_2O_3 based memristive device fabricated by dual ion beam sputtering," *Nanotechnology* **29**, 055203 (2018).
- W. Cranton, D. Spink, R. Stevens, and C. Thomas, "Growth and dielectric characterization of yttrium oxide thin films deposited on Si by rf-magnetron sputtering," *Thin Solid Films* **226**, 156–160 (1993).
- S. Y. Chiam, W. K. Chim, C. Pi, A. C. H. Huan, S. J. Wang, J. S. Pan, S. Turner, and J. Zhang, "Band alignment of yttrium oxide on various relaxed and strained semiconductor substrates," *J. Appl. Phys.* **103**, 083702 (2008).
- K. Z. Rushchanskii, S. Blügel, and M. Ležaić, "Ab initio phase diagrams of Hf-O, Zr-O, and Y-O: A comparative study," *Faraday Discuss.* **213**, 321–337 (2019).
- S. U. Sharath, S. Vogel, L. Molina-Luna, E. Hildebrandt, C. Wenger, J. Kurian, M. Duerrschabel, T. Niermann, G. Niu, P. Calka, M. Lehmann, H.-J. Kleebe, T. Schroeder, and L. Alff, "Control of switching modes and conductance quantization in oxygen engineered HfO_x based memristive devices," *Adv. Funct. Mater.* **27**, 1700432 (2017).
- S. Petzold, A. Zintler, R. Eilhardt, E. Piros, N. Kaiser, S. U. Sharath, T. Vogel, M. Major, K. P. McKenna, L. Molina-Luna, and L. Alff, "Forming-free grain boundary engineered hafnium oxide resistive random access memory devices," *Adv. Electron. Mater.* **5**, 1900484 (2019).
- E. Piros, M. Lonsky, S. Petzold, A. Zintler, S. U. Sharath, T. Vogel, N. Kaiser, R. Eilhardt, L. Molina-Luna, C. Wenger, J. Müller, and L. Alff, "Role of oxygen defects in conductive-filament formation in Y_2O_3 -based analog RRAM devices as revealed by fluctuation spectroscopy," *Phys. Rev. Appl.* (in press).
- B. Lacroix, F. Paumier, and R. J. Gaboriaud, "Crystal defects and related stress in Y_2O_3 thin films: Origin, modeling, and consequence on the stability of the C-type structure," *Phys. Rev. B* **84**, 014104 (2011).
- C. Vallée, P. Gonon, C. Jorel, F. E. Kamel, M. Mougenot, and V. Jousseume, "High k for MIM and RRAM applications: Impact of the metallic electrode and oxygen vacancies," *Microelectron. Eng.* **86**, 1774–1776 (2009).
- I. Valov, "Interfacial interactions and their impact on redox-based resistive switching memories (ReRAMs)," *Semicond. Sci. Technol.* **32**, 093006 (2017).
- D. Basak and S. Sen, "Electrical, dielectric and optical properties of $M/Y_2O_3/M$ devices," *Thin Solid Films* **254**, 181–186 (1995).
- M. Zhu, X. Li, X. Li, X. Zang, Z. Zhen, D. Xie, Y. Fang, and H. Zhu, "Schottky diode characteristics and 1/f noise of high sensitivity reduced graphene oxide/Si heterojunction photodetector," *J. Appl. Phys.* **119**, 124303 (2016).
- K. Hattori and Y. Torii, "A new method to fabricate Au/N-type InP Schottky contacts with an interfacial layer," *Solid-State Electron.* **34**, 527–531 (1991).
- J. H. Werner and H. H. Güttler, "Barrier inhomogeneities at Schottky contacts," *J. Appl. Phys.* **69**, 1522–1533 (1991).

- ²⁷P. Mundt, S. Vogel, K. Bonrad, and H. von Seggern, "Inverse I-V injection characteristics of ZnO nanoparticle-based diodes," *ACS Appl. Mater. Interfaces* **8**, 20168–20175 (2016).
- ²⁸D. Reddy, M. Reddy, N. Reddy, and V. Reddy, "Schottky barrier parameters of Pd/Ti contacts on N-type InP revealed from I-V-T and C-V-T measurements," *J. Mod. Phys.* **2**, 113–123 (2011).
- ²⁹V. Y.-Q. Zhuo, Y. Jiang, and J. Robertson, "Thermal stability investigation in highly-uniform and low-voltage tantalum oxide-based RRAM," in 14th Annual Non-Volatile Memory Technology Symposium (NVMTS) (2014), pp. 1–4.
- ³⁰Z. Fang, H. Y. Yu, W. J. Liu, Z. R. Wang, X. A. Tran, B. Gao, and J. F. Kang, "Temperature instability of resistive switching on HfO_x-based RRAM devices," *IEEE Electron Device Lett.* **31**, 476 (2010).
- ³¹L. Putilov, A. Varaksin, and V. Tsidilkovski, "Defect formation and water incorporation in Y₂O₃," *J. Phys. Chem. Solids* **72**, 1090–1095 (2011).